

ASSESSING THE THIES LPM AERODYNAMIC BEHAVIOUR USING CFD SIMULATION AND WIND TUNNEL EXPERIMENTS

Enrico Chinchella^{1,2,*}, Arianna Causeruccio^{1,2}, Mattia Stagnaro & Luca G. Lanza^{1,2}

(1) Department of Civil, Chemical and Environmental Engineering, University of Genova, 16126 16145 Genova, Italy

(2) WMO Lead Centre "B. Castelli" on Precipitation Intensity, 16145 Genova, Italy

*email: enrico.chinchella@unige.it

KEY POINTS

- Wind induced airflow pattern near the Thies LMP precipitation gauge.
- Wind tunnel experiments to validate CFD numerical simulations.
- Impact of wind direction on non-catching precipitation gauges.

1 INTRODUCTION

A wide range of instruments are used to measure precipitation data. Non-Catching Gauges (NCGs) are being increasingly adopted by national weather services. NCGs differ from traditional catching-type gauges because they do not collect rainwater in a container but sense each hydrometeor individually. By using indirect methods based on laser beams, optical imaging, impact transducers, and acoustic or radar sensors, they often allow the joint detection of the hydrometeor size and fall velocity. NCGs have a more complex, often non-axisymmetric shape because of the geometric constraints imposed by their measuring principle, nevertheless they have several advantages over traditional ones. The most relevant factors still preventing a widespread diffusion of NCGs are the lack of standardised calibration procedures and correction algorithms to compensate for instrumental and environmental biases (Lanza *et al.*, 2021).

Wind is the primary source of environmental biases for precipitation gauges, due to the so-called exposure effect. The gauge body, once impacted by wind, produces strong velocity gradients, vertical components, and the development of turbulence close to its surface, see, e.g., (Causeruccio *et al.*, 2021, Colli *et al.*, 2018). Trajectories of approaching hydrometeors are affected by these wind field features and can be deflected or have their fall velocity changed, introducing therefore some measurement bias, simply because of the presence of the instrument itself (invasive measurement). The non-axisymmetric shape of the gauge implies a dependency of the aerodynamic behaviour on the wind direction. Field comparisons, like the work of Upton and Brawn (2008), show that, even at limited wind speed, two such instruments installed with two different orientations (rotated by 90°) may report differences of up to 20% in the total number of detected hydrometeors. This suggests that the wind direction, further than the wind speeds, also affects their operational performance. To quantify the airflow deformation near the gauge, numerical simulation, based on computational fluid dynamics (CFD), can be employed (Něspor *et al.*, 2000). In this work, the Laser Precipitation Monitor (LPM), manufactured by Thies Inc. (Fig. 1a), is studied by means of numerical simulations, suitably validated through wind tunnel experiments.



Figure 1. In panel (a) the Thies LPM, with the emitting head (attached to the circuitry box on the left-hand side) and the receiving head (attached to the supporting arms on the right-hand side). In panel (b) an example of computational mesh used.

2 METHODOLOGY

2.1 CFD simulations

In this work, the OpenFOAM software was used to simulate the airflow pattern near the Thies LPM. Various undisturbed wind velocity values were tested, also changing the incoming wind direction to consider the effect of the non-axial symmetry of the instrument. Additionally, the supporting pole was included in the computational domain, since for some wind directions it may have an influence on the airflow velocity magnitude and direction near the sensing area. A numerical model of the Thies LPM, including the supporting pole, was realised in the Standard Triangulation Language (STL) format. The computational mesh was produced within OpenFOAM, for a 4 m long, 2.4 m wide, and 2 m high simulation domain (Fig. 1b). The origin of the reference system is in the centre of the sensing area. The internal mesh has a maximum cell size of 0.04 m and is progressively refined to reproduce the finer geometrical details and to correctly simulate turbulence. The direction of the incoming wind was set parallel to the X axis, while nine different meshes were realized after rotating the instrument, from $\alpha = 0^\circ$ to $\alpha = 180^\circ$ with increments of 22.5° . For the nine wind directions investigated, the final mesh contains between four and five million cells. Finally, for each wind direction, five wind speed values (U_{ref}) equal to 2, 5, 10, 15, and 20 m/s were tested for a total of 45 simulated wind direction/velocity configurations. In this work, the $k-\omega$ Shear Stress Transport (SST) turbulence model is used, where k is the turbulent kinetic energy and ω the specific turbulent dissipation rate. Simulations were conducted considering air as incompressible, with a density of 1.0 kg/m^3 and a kinematic viscosity of $1.5 \times 10^{-5} \text{ m}^2/\text{s}$. The free stream turbulence intensity was set equal to 1%. The Unsteady Reynolds-Averaged Navier–Stokes (URANS) equations were numerically solved using a pseudo-transient approach, based on a local time stepping (LTS) numerical scheme (Jeanmasson et al., 2019).

2.2 Wind tunnel experiments

Simulations were then validated by using wind tunnel (WT) measurements, conducted in the facility of the Department of Civil, Chemical and Environmental Engineering (DICCA) of the University of Genova. A multi-hole pressure probe, called “Cobra”, attached to a traversing arm, provided the three velocity components of the flow. A full-scale Thies LPM instrument was installed on its supporting pole in the WT, fixed to a rotating baseplate. By rotating the instrument, each of the nine wind directions simulated, was reproduced in the WT. For each rotation, the airflow velocity was set equal to 5 and 10 m/s. For each position, measurements were taken at a frequency of 1000 Hz for 30 s. In total, 915 flow velocity measurements were obtained for nine rotations and two undisturbed airflow velocities.

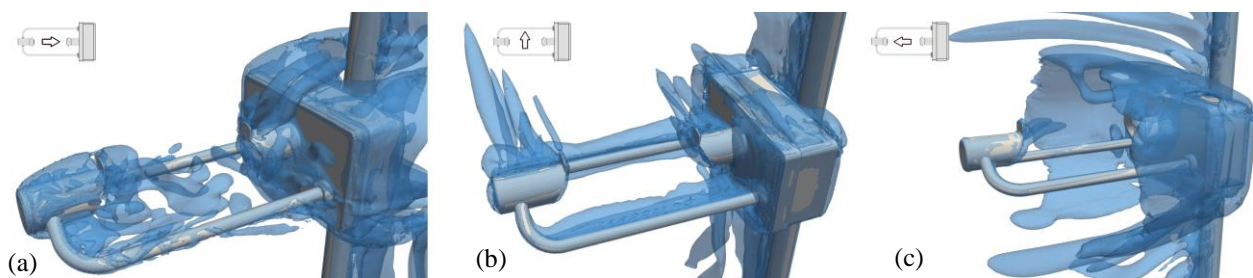


Figure 2. Visualization of the turbulent structures around the instrument using the Q-criterion at $U_{ref} = 10 \text{ m/s}$ and $\alpha = 0^\circ, 90^\circ$, and 180° in the a, b and c panels, respectively.

3 RESULTS

3.1 Numerical simulations

The vortex structures near the instrument body are visualized in Figure 2 by means of the Q-criterion. At $\alpha = 0^\circ$ (2a), the wake generated by the receiving head strongly affects the sensing area of the instrument and the flow region above it. At $\alpha = 90^\circ$ (2b), neither the turbulence structures produced by the two heads and the circuitry box, nor the turbulent wake from the supporting arm affect the sensing area. At $\alpha = 180^\circ$ (2c), the

circuitry box produces large vortex structures that completely envelop the instrument sensing area. Wind velocity maps are presented considering the (X, Z) section of the flow field at $Y=0$, for $U_{ref} = 10$ m/s. Figures 3a, 3d and 3g show the horizontal velocity while the vertical velocity is shown in figures 3b, 3e and 3h, finally in figures 3c, 3f and 3i, the turbulence kinetic energy is presented. At $\alpha = 0^\circ$, the receiver head is the first obstacle to the flow, producing accelerated zones and vertical velocity components above and below the sensing area of the instrument (white horizontal line), and a recirculation zone just downstream of the obstacle, with reduced velocity and high turbulence. At $\alpha = 90^\circ$, the flow near the sensing area is mostly undisturbed, the shedding of vortices generated by the supporting arms produces only a limited influence on the velocity magnitude, while recirculation zones are concentrated near the receiving head, the instrument box, and the emitting head. Turbulence close to the laser beam is minimal. At $\alpha = 180^\circ$, the circuitry box acts as a large obstacle for the flow and, together with the supporting pole, generates a large recirculation zone. Above the sensing area, two zones of first accelerated and then decelerated flow are present, with a considerable updraft and generation of turbulence due to the recirculation effect. Similar results were obtained for the other velocities, recirculation, and vertical velocity components non-linearly decrease from the 0° configuration to the 90° configuration, where a minimum is reached, and then increase again approaching the 180° configuration, where the maximum amount of flow disturbance is obtained.

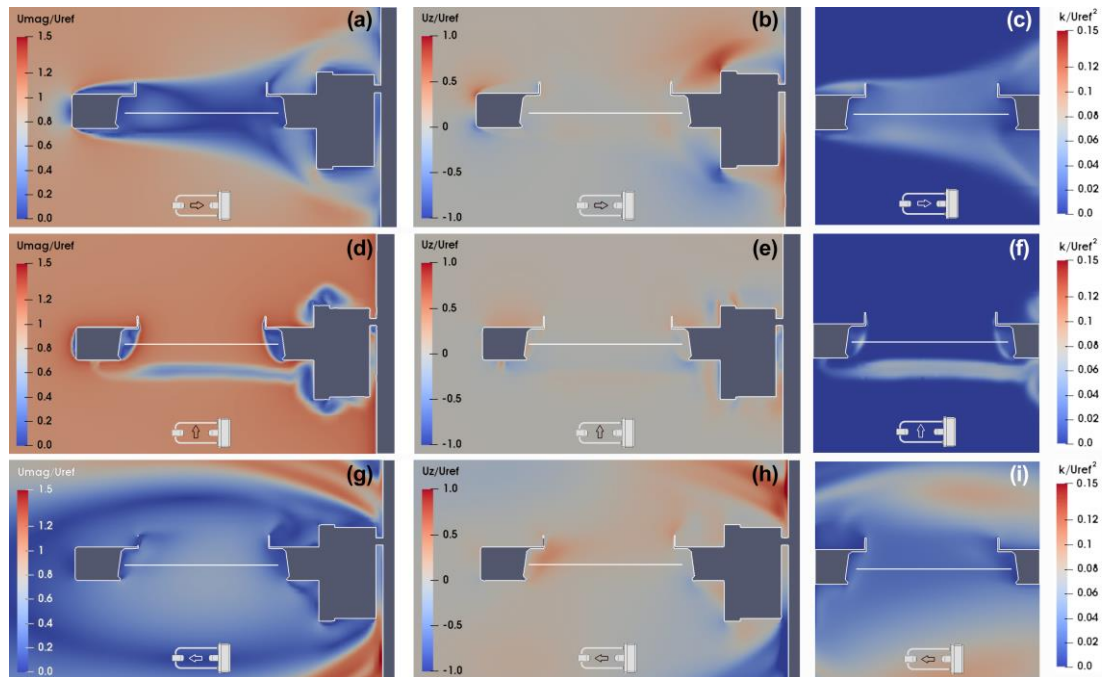


Figure 3. CFD simulation at $U_{ref} = 10$ m/s and $\alpha = 0^\circ$ (a, b, c), $\alpha = 90^\circ$ (d, e, f) and $\alpha = 180^\circ$ (g, h, i). Maps of the normalized magnitude U_{mag}/U_{ref} (a, d, g), vertical component U_z/U_{ref} (b, e, h) and normalized turbulent kinetic energy (k/U_{ref}^2) (c, f, i), along the (X, Z) section of the flow field at $Y = 0$. The white horizontal line indicates the position of the sensing area of the instrument, while the small arrow indicates the undisturbed flow direction.

3.2 Wind tunnel validation

Due to the large number of measurements taken, a statistical approach was used for validation: in this analysis only those measurements satisfying some minimum quality criteria were used. Under the hypothesis of a Gaussian distribution of measurement errors, 95.45% of the points are expected to be within 2σ , while 99.73% should be within 3σ , with σ being the instrument accuracy (0.5 m/s). Observing the results in Table 1, most rotations satisfy this criterion, although with a few outliers. These could be explained by the fact that some points are very close to the quality threshold used and that the presence of the probe itself locally modifies the velocity field, especially near the surface of the instrument. Additionally, because of the limited number of usable data for some angles, one single outlier could have a strong influence on the test result.

Wind dir.	Mean Error [m/s]		Std. Dev. [m/s]		% Out of Tolerance		% Data within 2σ		% Data within 3σ		
	U_{ref}	5m/s	10m/s	5m/s	10m/s	5m/s	10m/s	5m/s	10m/s	5m/s	10m/s
0°	0.376	0.370	0.554	0.590	25.00	33.33	83.33	75.00	95.83	91.67	
22.5°	0.345	0.410	0.538	0.351	12.00	15.79	92.00	92.11	92.00	97.37	
45°	0.117	0.098	0.267	0.147	2.22	0.00	97.78	100.00	97.78	100.00	
67.5°	0.103	0.157	0.192	0.280	4.08	4.44	100.00	97.78	100.00	100.00	
90°	0.084	0.139	0.156	0.218	1.56	4.69	98.44	98.44	100.00	100.00	
112.5°	0.102	0.121	0.245	0.151	2.22	0.00	97.78	100.00	97.78	100.00	
135°	0.228	0.236	0.448	0.256	15.63	6.67	90.63	96.67	96.88	100.00	
157.5°	0.322	0.540	0.446	0.758	10.53	27.78	94.74	83.33	100.00	88.89	
180°	1.806	3.722	1.185	0.879	33.33	100	58.33	0.00	75.00	0.00	

Table 1. Statistical validation of the numerical simulations against the WT measurements.

4 CONCLUSIONS

Simulation results show that wind direction is the primary factor dictating the airflow pattern near the Thies LPM. The airflow near the sensing area changes considerably and, in some cases, abruptly with the wind direction, demonstrating a strongly non-linear behaviour. Depending on the wind direction, the normalised average updraft is between 3% and 10% (with peak velocities up to 70% of the freestream value), while the downdraft is between 2% and 16% (with peaks up to 40%). The horizontal velocity also increases significantly, up to 27%, and even reverses its direction (with values up to 55%) due to the induced recirculation. Transversal velocity components are also present, with peak values up to 88% and average values up to 10%. These strong velocity gradients near the instrument body are non-negligible and potentially affect the approaching hydrometeors. The configuration for $\alpha = 90^\circ$ presents the minimum airflow disturbance and therefore it is expected that it would introduce the least amount of bias in measurements taken under the influence of wind. Angles close to 90° also present favourable results while the configurations at 0° and especially 180° are the worst performing ones, with the latter producing the strongest disturbance. The occurrence of such configurations should be minimised in field installations, and extreme care should be taken in analysing measurements taken in such conditions, since the associated wind-induced bias is expected to be significant. The proposed airflow numerical simulation framework provides a basis to develop correction curves for the wind-induced bias of NCGs, depending not only on the undisturbed wind speed and precipitation intensity, but also on the wind direction.

REFERENCES

- Cauteruccio, A., Brambilla, E., Stagnaro, M., Lanza, L.G. & Rocchi, D. Experimental evidence of the wind-induced bias of precipitation gauges using Particle Image Velocimetry and particle tracking in the wind tunnel. *J. Hydrol.* 2021, 600(12), 126690
- Colli, M., Pollock, M., Stagnaro, M., Lanza, L.G., Dutton, M. & O’Connell, P.E. A Computational Fluid-Dynamics assessment of the improved performance of aerodynamic raingauges. *Water Resources Research* 2018, 54, 779–796
- Jeanmasson, G., Mary, I. & Mieussens, L. On some explicit local time stepping finite volume schemes for CFD. *Journal of Computational Physics*, 2019, 397, 108818
- Lanza, L.G., Merlone, A., Cauteruccio, A., Chinchella, E., Stagnaro, M., Dobre, M., Garcia Izquierdo, M.C., Nielsen, J., Kjeldsen, H., Roulet, Y.A., et al. Calibration of non-catching precipitation measurement instruments: A review, *Journal of Meteorological Applications*, 2021, 28, e2002
- Něsper, V., Krajewski, W.F. & Kruger, A. Wind-Induced Error of Raindrop Size Distribution Measurement Using a Two-Dimensional Video Disdrometer. *Journal of Atmospheric and Oceanic Technology*. 2000, 17, 1483–1492
- Upton, G. & Brawn, D. An investigation of factors affecting the accuracy of Thies disdrometers. In *Proceedings of the WMO/CIMO Technical Conference (TECO-2008)*, St. Petersburg, Russian Federation, 27–29 November 2008, pp. 27–29

Acknowledgements

This work is funded as part of the activities of the EURAMET project 18NRM03—“INCIPIT—Calibration and Accuracy of Non-Catching Instruments to measure liquid/solid atmospheric precipitation”.

This work was published as: Chinchella, E., Cauteruccio, A., Stagnaro, M. & Lanza, L. G., Investigation of the Wind-Induced Airflow Pattern Near the Thies LPM Precipitation Gauge. *Sensors*, 2021, 21(14), 4880.